Spin-Wave versus Joule Heating in Spin-Hall-Effect/Spin-Transfer-Torque Driven Cr|Heusler|Pt Waveguides

T. Meyer,[1] T. Brächer,[1,2] F. Heussner,[1] A.A. Serga,[1] H. Naganuma,[3]
K. Mukaiyama,[3] M. Oogane,[3] Y. Ando,[3] B. Hillebrands,[1] and P. Pirro[1]

[1] *Fachbereich Physik and Landesforschungszentrum OPTIMAS, Technische Universität Kaiserslautern, 67663 Kaiserslautern, Germany*

[2] *current affiliation: Université Grenoble Alpes, CNRS, CEA, INAC-SPINTEC, 38054 Grenoble, France*

[3] *Department of Applied Physics, Graduate School of Engineering, Tohoku University, Sendai 980-8579, Japan*

(Dated: December 3, 2024)

We present a time-resolved study of the DC-current driven magnetization dynamics in a microstructured Cr|Heusler|Pt waveguide by means of Brillouin light scattering. A reduction of the effective spin-wave damping via the spin-transfer-torque effect leads to a strong increase in the magnon density. This is accompanied by a decrease of the spin-wave frequencies. By evaluating the time scales of these effects, we find that the frequency shift can be attributed to a heating of the magnetic layer. Further investigations reveal that this heating is dominantly caused by the decay of spin waves which is accompanied by a flow of energy from the spin-wave system to the phonon system. In contrast, Joule heating due to the electric current and nonlinear effects only play a minor role. The results show that in any magnetic system which is strongly excited by the spin-transfer-torque effect the contribution to the temperature increase by an increased magnon density needs to be considered.

In the last years, the field of magnon spintronics has attracted a prominent interest as it offers the great potential to realize future logic devices based on wave computing. In this field, currents of magnons, the quanta of spin waves, are used to transport and process information. Recently a set of prototype devices have been realized such as, e.g., the magnon transistor [1], which allows to fully control a flow of magnons by other magnons. Another example is the magnonic majority gate [2, 3], in which the output signal is determined by the majority of the input signals. Especially the latter shows the power of wave computing using the spin-wave phase. Other works on magnon based devices such as the spin-wave multiplexer [4], domain walls as spin-wave nanochannels [5] or graded-index magnonics [6] pave the way towards a controlled spin-wave transfer in magnonic networks.

At the same time, the spin-transfer-torque (STT) effect [7] of a spin current, which is injected into a magnetic layer, enables the manipulation and excitation of magnetization dynamics. The influence of this torque is described by a modified Landau-Lifshitz and Gilbert equation and can be co-aligned with the Gilbert damping torque. This results in an effective spin-wave damping given by the interplay of the Gilbert damping parameter [8] and the STT effect. This lead, e.g., to the development of spin-torque nano-oscillators based on point-contacts which allow to generate oscillations in the GHz-range by DC currents [9, 10]. Furthermore, in combination with the spin-Hall-effect (SHE) [11] which converts a charge current into a spin current in a normal metal, the STT effect allows for the control of the effective spin-wave damping also in spatially extended magnonic devices [12–17]. To minimize the needed current densities and to achieve large STT-induced effects, a combination with new materials with a low spin-wave damping is very promising. Cobalt-based Heusler compounds are one candidate for such a material [18]. Using the SHE, e.g. in a Pt layer adjacent to the cobalt-based Heusler compound, the STT-effect offers a powerful link to combine magnonics with conventional CMOS technologies.

Up to now, most of the reported studies on the manipulation of spin waves in a magnonic waveguide via the SHE and the STT effect only use static DC currents or comparably long quasi-DC pulses with pulse durations of several microseconds. On this time scale, the spin-wave dynamics reach a quasi-equilibrium state as the lifetimes of magnons are in the range of a few nanoseconds. To investigate the transitional dynamics regime, DC pulses with a duration of several nanoseconds need to be applied. In this short pulse regime, the spin-wave response may differ from the case of long pulses or static currents since nonlinear magnon-magnon interactions might be less pronounced. Thus, the main focus of the presented work is on the temporal dependence of the spin-wave response on 50 ns long current pulses which results in a modulation of the effective spin-wave damping via the SHE and the STT effect. Investigations on the time evolution of the magnon density and the frequency of the observed spin waves reveal that the magnetic system is strongly heated only if the effective spin-wave damping is reduced by the injected spin current. Furthermore, a comparison of the measurements with simulations of the heat dissipation rate shows that the decaying spin waves themselves are the source of this heating. In contrast, Joule heating by the charge current only has a small influence.

In this Letter, we employ time-resolved Brillouin light scattering (BLS) microscopy [19] to observe the pulsed DC-current driven spin-wave dynamics in a spin-wave

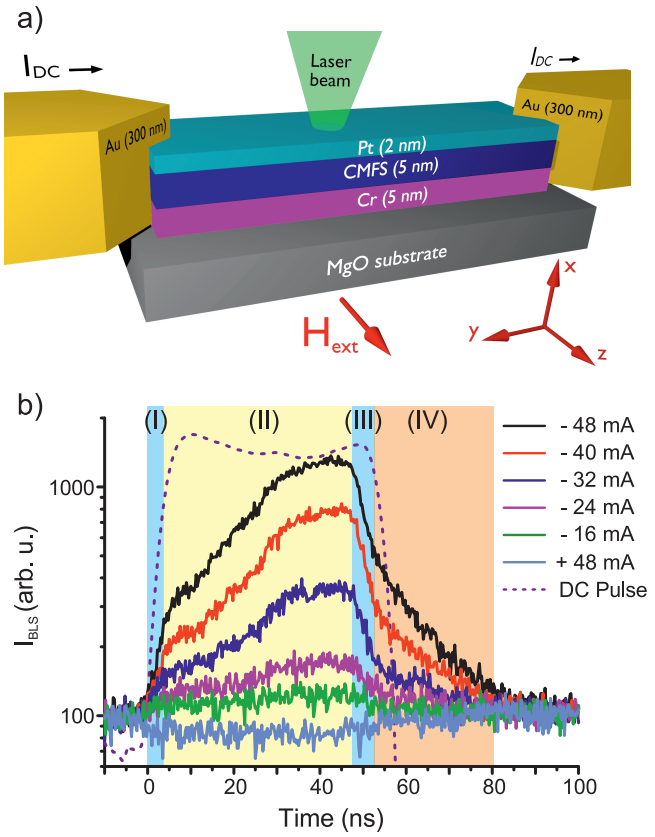

FIG. 1. (color online) a) Sketch of the investigated sample and the used coordinate system. The 7 μm wide and 30 μm long waveguide consists of a 5 nm thick Cr buffer layer, a 5 nm CMFS layer and a 2 nm Pt layer on top. 300 nm thick Au contacts at each end allow for the application of a DC current to the layer stack. The magnetization is aligned along the z-direction. b) Time evolution of the BLS intensity I_{BLS} for 50 ns long applied DC pulses and different current values (please note the log-scale). For large negative currents, a strong increase of the magnon density can be observed, whereas for positive currents the intensity is suppressed. The dashed line indicates the shape of the DC pulse.

waveguide. The magnetic layer of the 7 μm wide and 30 μm long waveguide is made from the low-damping Heusler compound $Co_2Mn_{0.6}Fe_{0.4}Si$ (CMFS) [20] (see Fig. 1a). To support the crystalline growth of the CMFS layer, a 5 nm thick Cr layer is deposited on a MgO substrate, acting as a buffer layer, since the magnetic properties of the CMFS layer strongly depend on its crystalline order. After an annealing step at a temperature of 700 °C, a 5 nm thick CMFS layer is grown on top of the Cr buffer layer. A second annealing step at a temperature of 500 °C is used to improve the crystalline order of the CMFS layer. Finally, a Pt layer of 2 nm thickness is deposited. The subsequent microstructuring into waveguides is performed by means of electron beam lithography and ion beam etching. In order to manipulate the effective spin-wave damping in the waveguide via the SHE and the STT effect, 300 nm thick Au contacts are patterned at each end of the waveguide.

When applying a DC pulse to these contacts, the electric current flows through the trilayer along the y-direction and, via the SHE, generates a pure spin current flowing in the x-z-plane; for the definition of the coordinate system see Fig. 1a. The component of the spin current along the -x-direction is injected into the CMFS layer. By applying an external magnetic field $\mathbf{H}_{ext}$, the CMFS layer is always magnetized along the z-direction, i.e., along the short axis of the waveguide and perpendicular to the charge current direction. In this geometry, the injected spin current produces a torque on the precessing CMFS moments via the STT effect which is co-aligned with the Gilbert damping torque [21].

As all layers of the waveguide are metallic, the applied charge current will be distributed among all of them. Thus, not only the charge current in the Pt layer but also the current in the Cr layer will be partially converted into a pure spin current and both spin currents are subsequently injected into the CMFS layer. According to Ref. [22], Cr exhibits a negative spin-Hall angle (SHA) [23], whereas the SHA of Pt is positive. Due to this fact and since the spin currents emerging from the Pt and Cr layers enter the CMFS layer from opposite surfaces, both spin currents add up. In contrast, the Oersted fields induced in the CMFS layer by the electric currents flowing in the Pt and Cr layers have different signs. Since they are similar in magnitude, they do not influence the spin-wave properties significantly.

As mentioned before, the injected pure spin currents induce a change of the effective spin-wave damping. This reduced (increased) damping leads to a strong increase (decrease) of the thermal equilibrium magnon density which can be observed by means of BLS spectroscopy of the thermal magnons. In the measurements presented below, the probing laser spot with a diameter of approximately 400 nm is positioned in the center of the waveguide (see Fig. 1a).

Figure 1b shows the time-resolved BLS intensity for 50 ns long applied DC pulses with different current values measured for an external magnetic field of $\mu_0 H_{ext} = +70$ mT. Exemplarily, the shape of the transmitted current pulse is shown by the dashed line. In general, four distinct regimes of the DC-pulse induced spin-wave dynamics can be identified which are indicated by the shaded areas. Regimes (I) and (III) relate to the first and last approximately 5 ns of the DC pulse, respectively. Here, the BLS intensity rapidly changes, indicating the transition to a new state determined by a changed effective damping of the spin-wave system. The rise (fall) time of this transition is in the same order as the rise (fall) time of the current pulse, respectively. Thus, this transition happens on a faster time scale as the time-resolution of the experimental setup which is in the or-

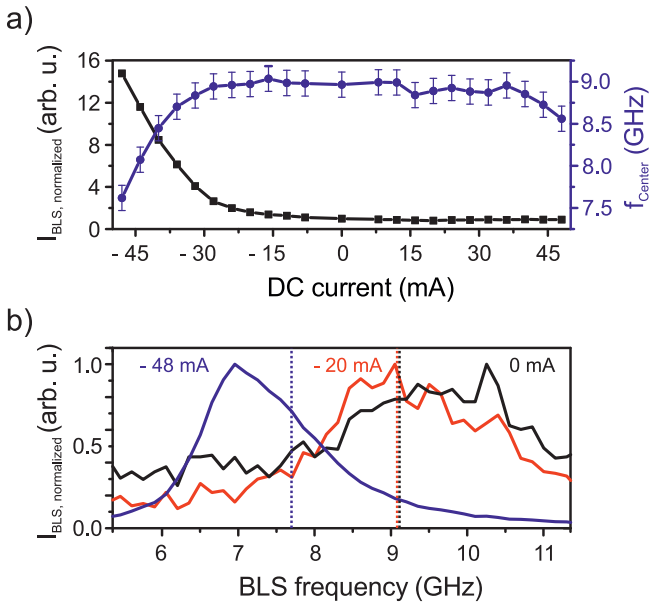

FIG. 2. (color online) a) The black squares show the integrated BLS intensity during the DC pulse as a function of the applied electric current, normalized to zero current. The corresponding center frequency of the spin-wave spectrum is depicted by the blue circles. b) Spin-wave frequency spectrum during the DC pulse for different applied currents. The dashed lines indicate the center frequency of the spectra.

der of 1 ns. Regime (II) corresponds to the time interval during which the applied DC current is approximately constant. Thus, also the torque acting on the magnetization is constant [24, 25]. Finally, regime (IV) describes the evolution of the BLS intensity after the current pulse.

The intensity increases in the case of negative applied currents which refers to a reduction of the effective spin-wave damping. In the presented system, the needed current value to compensate the damping is $I_{DC,Th} \approx -15$ mA. Thus, the highest applied current values significantly exceed the threshold resulting in a negative effective damping. It is worth to note that for positive applied currents, hence for an increase of the effective spin-wave damping, thermally excited spin waves can be suppressed [15] as exemplarily shown by the reduced intensity during the current pulse in Fig. 1b for an applied DC current of $I_{DC} = +48$ mA (blue curve).

The black squares in Fig. 2a show the BLS intensity $I_{BLS,\,normalized}$ during the DC pulse, integrated over the regimes (I)-(III) and over the whole observable spin-wave spectrum, normalized to the integrated BLS intensity in the absence of a current pulse. Here, the influence of the STT effect on the intensity of the spin waves is shown, which increases by more than a factor of 15 for negative applied currents. In addition, Fig. 2b exemplarily shows the observed spin-wave frequency spectrum during the DC pulse for different applied currents. For large negative currents (blue line) a pronounced shift of the spin-wave spectrum towards lower frequencies is observed. However, the frequency linewidth of the spin-wave excitation does not change significantly. This is in agreement with other reports [14, 15] and shows that the entire observed spin-wave spectrum is amplified via the STT effect. This fact is essential for a broadband amplification of propagating spin waves. This proves the ability of this technique to control the effective damping of propagating spin waves since no collapse of the spin-wave spectrum into a single mode is observed. The latter is the case for a confined system, see, e.g., Ref. 13.

The blue circles in Fig. 2a show the center frequency of the spin-wave spectrum depending on the applied current value. The center frequency is determined as the center of mass of the spectra as exemplarily depicted by the dashed lines in Fig. 2b. For large negative applied currents, a strong decrease of the frequency of approximately 1.5 GHz can be observed. In contrast, for positive currents, only at large applied current values a small frequency shift of approximately 0.5 GHz is detected.

In general, a lowering of the spin-wave frequency could be attributed to a reduction of the saturation magnetization. This could originate from a heating of the magnetic layer due to Joule heating of the DC current. However, Joule heating is proportional to $I_{DC}{}^2$, and, hence, only accounts for a symmetric lowering of the spin-wave frequency with the applied current. Thus, only the comparably small frequency shift for large applied positive currents might be caused by Joule heating. The significantly larger frequency shift at negative currents indicates that Joule heating only plays a minor role in this experiment.

Another possible origin of the observed asymmetric frequency shift is a nonlinear shift caused by the increased magnon density [26]. In this case, the frequency shift should be proportional to the magnon density rather than to show a simple proportionality to the applied current. To investigate the frequency shift in more detail, Fig. 3a exemplarily shows the time evolution of the BLS intensity (black curve) and the center frequency of the spin-wave spectrum (blue square) for an applied current pulse of −48 mA. In this case, the spin-wave damping is overcompensated, leading to a negative effective damping. Thus, in regime (II) in Fig. 3a, while the 50 ns long current pulse is applied, the magnon density constantly increases in time. During this intensity increase, a monotonous drop of the spin-wave frequency is observed which takes place on a similar time scale. In regime (III), when the current pulse is switched off, the magnon density quickly decreases within 5 ns. Since the magnon lifetime of about 1 ns is below the fall time of the pulse of about 5 ns, the observed intensity drop corresponds to the falling edge of the pulse. In contrast, the spin-wave frequency in regime (III) only shows a small change. This indicates that the aforementioned nonlinear shift cannot account for the origin of the shift of the spin-wave spec-

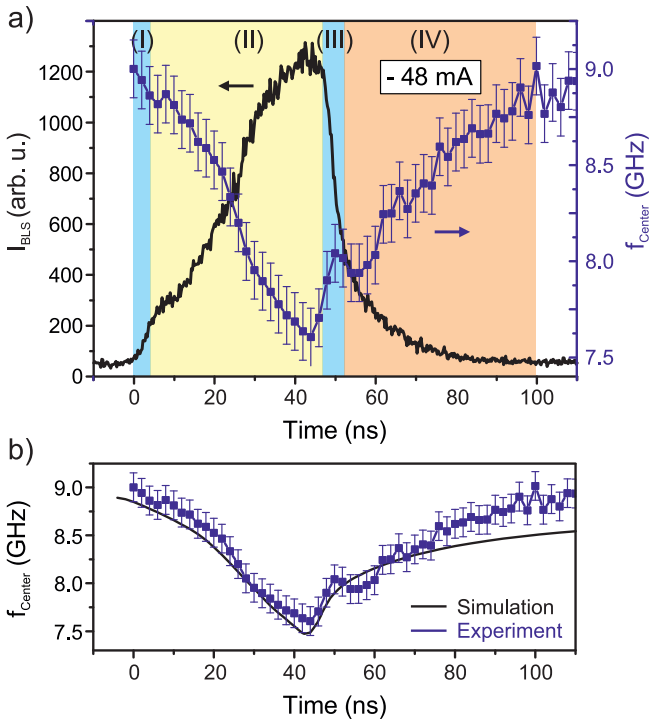

FIG. 3. (color online) Time evolution of the center frequency (blue squares) for a 50 ns long applied current pulse of −48 mA during regimes (I) - (III) in comparison to a) the spin-wave intensity (black line), and b) the simulated frequency shift (black line) induced by a spin-wave induced heating of the waveguide (black circles).

trum since the frequency shift does not follow the magnon density in regime (III) any more. Also a nonlinear shift due to exchange-dominated magnons, which could be excited via the STT effect but which are not accessible by the experimental setup, can be excluded. The observed dipolar-dominated magnons show much longer lifetimes compared to exchanged-dominated magnons at higher frequencies [27–29]. Thus, an influence of exchange-dominated magnons should lead to an even faster decay of the frequency shift after the current pulse.

Finally, in regime (IV), all magnons which were directly generated by the STT effect have already decayed. However, the frequency only slowly relaxes to the equilibrium value of approximately 9 GHz. The time scale for this frequency relaxation is in the order of several tens of nanoseconds. Also the residual magnon density in regime (IV) shows an exponential decay on a similar time scale, which is much larger than their lifetimes. This time scale of several tens of nanoseconds is a typical value for heat diffusion processes. This strongly indicates a heat induced shift of the spin-wave frequency and a small increase of the magnon density in regime (IV) due to a higher temperature of the CMFS layer. As already mentioned before, Joule heating only plays a minor role in the presented measurements. Thus, we conclude that the magnons themselves are the main source of heating.

To understand the heat generation by magnons during the current pulse, one needs to consider that the Gilbert damping is still present as a fundamental decay mechanism for magnons, even if the effective spin-wave damping is negative. This results in a flow of energy from the spin system into the phononic system, since magnon-electron interactions and subsequent electron-phonon scattering constitute the main spin-wave decay mechanisms in the investigated material. Thus, the temperature of the magnetic layer increases as the magnon density increases, resulting in a drop of the saturation magnetization and a lowering of the spin-wave frequency spectrum. It should be noted that the magnon density also partially increases due to the higher temperature itself which leads to the slow decay of the residual spin-wave intensity in regime (IV). However, as can be seen from the rapid drop of the magnon density in regime (III), this effect is small compared to the magnon density increase caused by the STT effect.

This effect of a spin-wave induced heating can explain the temporal behavior of the spin-wave intensity and the spin-wave frequency in all four regimes. In regime (II), the magnon density increases due to the STT effect and the short lifetimes of the magnons result in a fast temperature increase of the magnetic layer which causes a downshift of the spin-wave frequency. After the current pulse, i.e., in regimes (III) and (IV), the magnon density shows a rapid decay within the magnon lifetime. In contrast, the relaxation time of the spin-wave frequency is determined by the heat dissipation rate which constitutes a much slower relaxation process.

To verify the assumption that the frequency shift is induced by spin-wave heating, *COMSOL Multiphysics* simulations of the time evolution of the temperature of the magnetic layer have been performed [30, 33]. For this, a homogeneous heating of the CMFS layer with a time-dependent heating power is taken into account. The assumed heating power is proportional to the measured magnon density during the current pulse in regimes (I)-(II), followed by a 5 ns fall time to a vanishing heating power in regime (III). This heating results in a decrease of the saturation magnetization M_S of the CMFS which leads to the observed frequency shift. This shift of the spin-wave band approximately follows the shift of the ferromagnetic resonance frequency, which constitutes the origin of the spin-wave band and which is given by the Kittel formula [36]:

$$f(M_S(T)) = \gamma\sqrt{\mu_0 H_{ext}(\mu_0 H_{ext} + \mu_0 M_S(T))}. \quad (1)$$

Here, γ denotes the gyromagnetic ratio and H_{ext} denotes the externally applied magnetic field. The saturation magnetization of the unstructured Cr|Heusler|Pt film before the microstructuring could be determined to

$M_S \approx 1133$ kA/m by means of vibrating sample magnetometry. For an approximate description of the temperature-induced change of the magnetization, we assume a linear dependence $M_S(T) = M_S(1 - cT)$. The parameter c determines the strength of the saturation magnetization reduction with temperature and is the only parameter used to fit the frequency shift resulting from the simulated temporal evolution of the temperature in the CMFS layer to the experimentally obtained shift. The simulated frequency shift (black curve) as well as the measured frequency shift (blue squares) for an applied current of −48 mA are shown in Fig. 3b. The simulations indicate a decrease of the effective magnetization by up to 30 % during the pulse. In particular, the observed slow decay of the spin-wave frequency in regime (IV) is well reproduced. This relaxation time is given by the small heat dissipation rate and can be understood by considering that the MgO substrate has a rather small heat conductivity. As the layers of the waveguide are only 12 nm thick and 7 μm wide, a heat dissipation along the waveguide is suppressed. In addition, the probing laser is positioned in the center between the contacts and quite far away from these heat sinks. Hence, the probing spot is thermally well isolated which leads to the small heat dissipation rates. These results evidence that the spin-wave frequency shift is mainly caused by a heating of the magnetic layer by decaying spin waves.

In conclusion, we have shown that, by employing the SHE and the STT effect for the case of short applied current pulses, the effective spin-wave damping in the presented microstructured Cr|Heusler|Pt waveguide can be modulated in a wide range. Upon reducing the effective damping, a strong spin-wave frequency shift towards lower frequencies was observed alongside with a large increase of the spin-wave intensity. We have demonstrated that Joule heating and a nonlinear frequency shift only cause a minor contribution to the frequency shift in the investigated system. Time-resolved BLS measurements and COMSOL simulations revealed that decaying magnons lead to a temperature increase of the magnetic system resulting in a lowered spin-wave frequency. This shows that in any application using the STT effect, the contribution to the temperature increase by an increased magnon density needs to be considered.

The authors gratefully acknowledge financial support by the DFG in the framework of the research unit TRR 173 “Spin+X” and by the DFG Research Unit 1464 and the Strategic Japanese-German Joint Research Program from JST: ASPIMATT.

[1] A.V. Chumak, A.A. Serga, and B. Hillebrands, Nat. Commun. **5**, 1700 (2014).
[2] A. Khitun, M. Bao, and K.L. Wang, IEEE Trans. Magn. **44**, 2141 (2008).
[3] T. Fischer, M. Kewenig, D.A. Bozhko, A.A. Serga, I.I. Syvorotka, F. Ciubotaru, C. Adelmann, B. Hillebrands, A.V. Chumak, arXiv:1612.07708 (2016).
[4] K. Vogt, F.Y. Fradin, J.E. Pearson, T. Sebastian, S.D. Bader, B. Hillebrands, A. Hoffmann, and H. Schultheiss, Nat. Commun. **5**, 3727 (2014).
[5] K. Wagner, A. Kákay, K. Schultheiss, A. Henschke, T. Sebastian, and H. Schultheiss, Nat. Nanotechnol. **11**, 432 (2016).
[6] C.S. Davies, A. Francis, A.V. Sadovnikov, S.V. Chertopalov, M.T. Bryan, S.V. Grishin, D.A. Allwood, Y.P. Sharaevskii, S.A. Nikitov, and V.V. Kruglyak, Phys. Rev. B **92**, 020408 (2015).
[7] J.C. Slonczewski, J. Magn. Magn. Mater. **159** (1996).
[8] T.L. Gilbert, IEEE Trans. Magn. **40**, 3443 (2004).
[9] T.J. Silva, and W.H. Rippard, J. Magn. Magn. Mater. **320**, 1260 (2008).
[10] J.V. Kim, Solid State Physics **63**, 217 (2012).
[11] J. Hirsch, Phys. Rev. Lett. **83**, 1834 (1999).
[12] K. Ando, S. Takahashi, K. Harii, K. Sasage, J. Ieda, S. Maekawa, and E. Saitoh, Phys. Rev. Lett. **101**, 036601 (2008).
[13] V.E. Demidov, S. Urazhdin, H. Ulrichs, V. Tiberkevich, A. Slavin, D. Baither, G. Schmitz, and S.O. Demokritov, Nat. Mater. **11** (2012).
[14] M. Evelt, V.E. Demidov, V. Bessonov, S.O. Demokritov, J.L. Prieto, M. Muñoz, J. Ben Youssef, V.V. Naletov, G. de Loubens, O. Klein, M. Collet, K. Garcia-Hernandez, P. Bortolotti, V. Cros, and A. Anane, Appl. Phys. Lett. **108**, 172406 (2016).
[15] V.E. Demidov, S. Urazhdin, E.R.J. Edwards, M.D. Stiles, R.D. McMichael, and S.O. Demokritov, Phys. Rev. Lett. **107**, 107204 (2011).
[16] O. Gladii, M. Collet, K. Garcia-Hernandez, C. Cheng, S. Xavier, P. Bortolotti, V. Cros, Y. Henry, J.-V. Kim, A. Anane, and M. Bailleul, Appl. Phys. Lett. **108**, 202407 (2016).
[17] K. An, D.R. Birt, C.-F. Pai, K. Olsson, D.C. Ralph, R.A. Buhrmann, and X. Li, Phys. Rev. B **89**, 140405 (2014).
[18] S. Mizukami and A.A. Serga, J. Phys. D: Appl. Phys. **48**, 160301 (2015).
[19] T. Sebastian, K. Schultheiss, B. Obry, B. Hillebrands, and H. Schultheiss, Front. Phys. **3**, 35 (2015).
[20] T. Sebastian, Y. Ohdaira, T. Kubota, P. Pirro, T. Brächer, K. Vogt, A.A. Serga, H. Naganuma, M. Oogane, Y. Ando, and B. Hillebrands, Appl. Phys. Lett. **100**, 112402 (2012).
[21] I.N. Krivorotov, N.C. Emley, J.C. Sankey, S.I. Kiselev, D.C. Ralph, and R.A. Buhrmann, Science **307**, 228 (2005).
[22] C. Du, H. Wang, F. Yang, and P.C. Hammel, Phys. Rev. B **90**, 140407 (2014).
[23] M. Schreier, G.E.W. Bauer, V. Vasyuchka, J. Flipse, K. Uchida, J. Lotze, V. Lauer, A. Chumak, A.A. Serga, S. Daimon, T. Kikkawa, E. Saitoh, B.J. van Wees, B. Hillebrands, R. Gross, and S.T.B. Goennenwein, J. Phys. D **48**, 025001 (2014).
[24] In general, the spin-mixing conductance, and, consequently, the injected spin current and the torque on the magnetization are temperature dependent. However, in the following, the temperature dependence of the torque is neglected since all observed phenomena can be ex-

plained by the increased magnon density.
[25] K. Uchida, T. Kikkawa, A. Miura, J. Shiomi, and E. Saitoh, Phys. Rev. X **4**, 041023 (2014).
[26] P. Krivosik and C.E. Patton, Phys. Rev. B **82**, 184428 (2010).
[27] D.D. Stancil, and A. Prabhakar, *Spin Waves Theory and Applications*, Springer Science+Business Media LLC, New York (2009)
[28] K. Zakeri,m Y. Zhang, T.H. Chuang, and J. Kirschner, Phys. Rev. Lett. **108**, 197205 (2012).
[29] H.J. Qin, K. Zakeri, A. Ernst, L.M. Sandratskii, P. Buczek, A. Marmodoro, T.H. Chuang, Y. Zhang, J. Kirschner, Nat. Comm. **6**, 6126 (2015).
[30] The thermal properties of this CMFS compound are not known. Furthermore, the reported values for the related electric conductivity of the compound Co_2MnSi vary in a wide range [31, 32]. However, to allow for the presented estimation of the time scales for the heat dissipation, the parameters of another metal are used. However, for an estimation of the time scales of the heat dissipation, the use of the parameters of a similar metal are sufficient. In this case, for simplicity, we assume the same thermal parameters of the CMFS layer as for a Co layer.
[31] K. Kim, S.J, Kwon, and T.W. Kim, Phys. Rev. B **82**, 184428 (2010).
[32] L. Ritchie, G Xiao, Y. Ji, T.Y. Chen, C.L. Chien, M. Zhang, J. Chen, Z. Liu, G. Wu, and X.X. Zhang, Phys. Stat. Sol. (B) **241**, 1557 (2003).
[33] The COMSOL multiphysics simulations are performed using the following parameters for the density ρ, heat capacity c_p and thermal conductivity k:
MgO [34]: $\rho_{MgO} = 3580$ kg m^{-3}, $c_{p,MgO} = 877$ J kg^{-1}K^{-1}, $k_{MgO} = 38.5$ W m^{-1}K^{-1}.
Cr [35]: $\rho_{Cr} = 7190$ kg m^{-3}, $c_{p,Cr} = 461$ J kg^{-1}K^{-1}, $k_{Cr} = 69.1$ W m^{-1}K^{-1}.
Co [35]: $\rho_{Co} = 8800$ kg m^{-3}, $c_{p,Co} = 440$ J kg^{-1}K^{-1}, $k_{Co} = 69.2$ W m^{-1}K^{-1}.
Pt [35]: $\rho_{Pt} = 21450$ kg m^{-3}, $c_{p,Pt} = 134$ J kg^{-1}K^{-1}, $k_{Pt} = 69.1$ W m^{-1}K^{-1}.
Au [35]: $\rho_{Au} = 19320$ kg m^{-3}, $c_{p,Au} = 128$ J kg^{-1}K^{-1}, $k_{Au} = 301$ W m^{-1}K^{-1}
[34] Producer: Furuchi Chemical, Tokyo, Japan
[35] www.matweb.com
[36] C. Kittel, Phys. Rev. **73**, 2 (1948).